Published in final edited form as:
J Biomech. 2010 September 17; 43(13): 2574–2581. doi:10.1016/j.jbiomech.2010.05.011.

THE EFFECTS OF APONEUROSIS GEOMETRY ON STRAIN INJURY SUSCEPTIBILITY EXPLORED WITH A 3D MUSCLE MODEL

Michael R. Rehorn[a] and **Silvia S. Blemker, PhD**[a,b,*]

[a]Biomedical Engineering, University of Virginia, Charlottesville, VA, United States

[b]Mechanical and Aerospace Engineering, University of Virginia, Charlottesville, VA, United States

Abstract

In the musculoskeletal system, some muscles are injured more frequently than others. For example, the biceps femoris longhead (BFLH) is the most commonly injured hamstring muscle. It is thought that acute injuries result from large strains within the muscle tissue, but the mechanism behind this type of strain injury is still poorly understood. The purpose of this study was to build computational models to analyze the stretch distributions within the BFLH muscle and to explore the effects of aponeurosis geometry on the magnitude and location of peak stretches within the model. We created a three-dimensional finite element (FE) model of the BFLH based on magnetic resonance (MR) images. We also created a series of simplified models with a similar geometry to the MR-based model. We analyzed the stretches predicted by the MR-based model during lengthening contractions to determine the region of peak local fiber stretch. The peak along-fiber stretch was 1.64 and was located adjacent to the proximal myotendinous junction (MTJ). In contrast, the average along-fiber stretch across all the muscle tissue was 0.95. By analyzing the simple models, we found that varying the dimensions of the aponeuroses (width, length, and thickness) had a substantial impact on the location and magnitude of peak stretches within the muscle. Specifically, the difference in widths between the proximal and distal aponeurosis in the BFLH contributed most to the location and magnitude of peak stretch, as decreasing the proximal aponeurosis width by 80% increased peak average stretches along the proximal MTJ by greater than 60% while slightly decreasing stretches along the distal MTJ. These results suggest that the aponeurosis morphology of the BFLH plays a significant role in determining stretch distributions throughout the muscle. Furthermore, this study introduces the new hypothesis that aponeurosis widths may be important in determining muscle injury susceptibility.

Keywords

muscle mechanics; hamstrings; biceps femoris longhead; aponeurosis; along-fiber stretch; finite element model

Please send all correspondence to: Silvia S. Blemker, Ph.D., Department of Mechanical & Aerospace Engineering, University of Virginia, 122 Engineer's Way, P.O. Box 400746, Charlottesville, Virginia 22904-4746, Phone: 434-924-6291, Fax: 434-982-2037, ssblemker@virginia.edu.

Conflict of interest statement

We would like to declare that we do not have any conflict of interest to report in this research.

Introduction

Some skeletal muscles are injured more commonly than others (Garrett, 1999); however, the factors making certain muscles more injury prone are not well understood. For example, amongst the bilateral hamstring muscles, the biceps femoris longhead (BFLH) is injured most frequently, accounting for approximately 80% of all hamstrings injuries (Armfield et al., 2006). Previous investigations have reported that injury in the BFLH is most often observed along the length of the myotendinous junction (MTJ) in the proximal region of the muscle tissue (Clanton and Coupe, 1998; Koulouris and Connell, 2003; Silder et al., 2008). While these injury patterns are well documented, the underlying mechanisms that give rise to these patterns are not presently understood. It remains unclear why the BFLH is more prone to injury than the other hamstrings muscles and why injuries in the BFLH are generally localized near the proximal MTJ.

Strain injury in skeletal muscle has been thought to result when regions of a muscle experience localized strains above a certain threshold (Garrett, 1999). Those regions have been shown to correspond to the location of injury (Best et al., 1995). Muscles are most prone to injury while performing lengthening contractions (Armstrong et al., 1983; Faulkner et al., 1993; Lieber and Friden, 2002; Noonan and Garrett, 1992; Schwane and Armstrong, 1983) and the magnitude of lengthening strains correlates with the degree of fiber injury (Lieber and Friden, 1993). The BFLH and the other bilateral hamstrings undergo similar lengthening musculotendon strains and loading during running (Thelen et al., 2005b). One possible explanation for the BFLH's increased incidence for injury is that the muscle experiences larger localized strains as compared to the other hamstrings. Since BFLH injuries are more commonly located near the proximal MTJ, the localized strains would also likely be concentrated in this region.

What features of the internal architecture of the BFLH could give rise to large localized strains along the proximal MTJ? The muscle fibers of the BFLH originate along a long, narrow proximal aponeurosis and insert along a shorter, broader distal aponeurosis. Previous studies have established that aponeuroses perform important roles during locomotion (Azizi and Roberts, 2009; Roberts et al., 1997) and may also help protect muscles from injury by reducing overall fascicle strains during lengthening contractions (Lemos et al., 2008). While the effects of the aponeurosis on overall fiber stretch have been investigated, little is known about how aponeurosis morphology affects local tissue stretches. In order to investigate the effects of aponeurosis morphology on muscle tissue stretch distributions, a model that incorporates the complex shape and mechanical properties of the aponeuroses and muscle tissue is needed.

The purpose of this study was to build computational models to determine how the aponeurosis dimensions of the BFLH muscle influence stretch distributions in the muscle tissue. In order to determine if the three-dimensional morphology of the muscle gives rise to large stretches localized along the proximal MTJ, we developed a three-dimensional finite element (FE) model of the BFLH based on magnetic resonance (MR) imaging data. We analyzed stretch distributions within the FE model for a simulated activated lengthening condition. We also constructed a simplified BFLH model with muscle architecture and aponeurosis dimensions that matched those of the MR-based model. By varying the aponeurosis width, length, and thickness of the simplified model, we were able to determine how each aponeurosis dimension affects the stretch distributions within the muscle tissue.

Methods

MR-Based BFLH Model

We reconstructed the surface geometry of the BFLH muscle, proximal aponeurosis, distal aponeurosis, and femur from MR image data (Fig. 1A). A series of axial MR images were acquired of a healthy male subject's upper thigh in a 1.5-T MR scanner (General Electric Healthcare, Milwaukee, WI, USA) with a 3*mm* slice thickness (matrix, 512×512; field of view, 400×400*mm*). Images were acquired over the thigh from the BFLH origin to the BFLH insertion. In all images, the boundaries of the structures of interest were manually outlined using Mimics segmentation software (Mimics 12.0, Materialise NV). Three-dimensional polygonal surface reconstructions were created for each structure based on the axial segmentation data. We created a finite element mesh consisting of approximately 20,000 eight-node hexahedral elements of the BFLH muscle based on these surface reconstructions using the FE mesh generator TrueGrid (XYZ Scientific Applications, Livermore, CA) (Fig. 1B). Aponeurosis and muscle tissue were constrained to remain attached to one another by defining tied contact interface between coinciding nodes (Puso et al., 2006).

In order to define the corresponding fiber geometry for the BFLH model, we used a mapping technique that applies muscle specific fiber architecture to the FE mesh (Blemker and Delp, 2005). The fiber map was defined such that the fibers originated along the proximal aponeurosis and inserted along the distal aponeurosis (Fig. 1C). Based on the fiber map, a fiber direction vector was determined for each element in the mesh to serve as an input to the constitutive model. The average fiber length for the BFLH fiber map was 10.5*cm*, which agrees well with reported values for the BFLH muscle (Ward et al., 2009).

Simple BFLH Model

In order to explore the effects of aponeurosis morphology on the stretch distributions within the MR-based BFLH model, we constructed a series of simplified finite element models. These models all had a simplified geometry that was based on anatomical measurements from the MR-based model. This approach allowed us to independently isolate the effects of the aponeurosis dimensions on stretches within the muscle tissue.

To define the dimensions of the simple models, we made several measurements from the MR-based BFLH model. The first set of dimensions was the same across all model variations; these included: overall BFLH muscle-tendon length, the lengths of the proximal and distal external tendons, and the average distance between the proximal and distal aponeuroses. The second set of dimensions was used to define the morphology of the aponeuroses in what will be referred to as the "simple BFLH model" (Fig. 2B): aponeurosis length, thickness, and width. We measured proximal and distal aponeurosis lengths of 17.8*cm* and 15.6*cm* respectively. These measurements were in good agreement with published data for the same muscle (Woodley and Mercer, 2005). In order to determine the thickness of the proximal and distal aponeuroses, we measured the aponeurosis thickness on multiple axial MR images. The average thickness along the length of each individual MTJ (Fig. 2A) was used to define the thickness in the simple model (Fig. 2B). The proximal aponeurosis had a measured thickness of approximately 3*mm* and the distal aponeurosis was thinner with an average thickness of approximately 1*mm*. Finally, we measured the widths of the proximal and distal aponeuroses across multiple axial MR images and found an average width of approximately 8*mm* for the proximal aponeurosis and approximately 40*mm* for the broader distal aponeurosis. These measurements were used to define the baseline simple BFLH model for comparison with the MR-based BFLH model. Fiber maps were defined such that fibers ran from the proximal aponeurosis to distal aponeurosis.

Simple Model Variations

Using variations on the simple BFLH model, we conducted a sensitivity analysis to explore the effects of aponeurosis length, aponeurosis thickness, and aponeurosis width on stretch distributions within the model. Variation I had proximal and distal aponeuroses with equal widths and equal lengths. Successive model iterations were created by independently changing the length, thickness, and width of the two aponeuroses in order to explore which aponeurosis dimension had the greatest impact on stretch distributions within the model (Table 1).

Constitutive Model

In all models, muscle and tendon tissues were represented as transversely isotropic, hyperelastic, quasi-incompressible materials. The strain energy density function was defined as:

$$\Phi = W_1(\lambda, act) + W_2(\varphi) + W_3(\phi) + U(J), \tag{1}$$

where λ, act, φ, ϕ, and J represent fiber stretch, activation level, along-fiber shear strain, cross-fiber shear strain and volume strain, respectively (Blemker et al., 2005; C. Criscione et al., 2001; Weiss et al., 1996). W_1 is a function of activation level and fiber length and therefore is dependent on the force length relationship of a sarcomere (Zajac, 1989). Activation level is input into the model and can vary with time between 0 (passive) and 1 (maximum voluntary contraction) throughout the course of a simulation. Stress and strain are related by:

$$\boldsymbol{S} = 2\frac{\partial \Phi}{\partial \mathbf{C}}, \tag{2}$$

where **S** is the Second Piola-Kirchoff stress tensor and **C** is the Right Cauchy-Green deformation tensor. A thorough description of the constitutive model has been previously published in Blemker et al. 2005 (Blemker et al., 2005).

Model Simulations

All model simulations were conducted using the implicit nonlinear finite element solver Nike3D (Puso et al., 2006). Lengthening contractions were simulated by applying a muscle-tendon lengthening in linear increments from 0*cm* to 2*cm* (which corresponds to roughly 40 degrees of knee extension motion) while linearly increasing the activation level from 0.1 to 0.5 during the course of lengthening. In all simulations, the proximal external tendon was fixed at its point of origin and displacement was prescribed to the distal external tendon. We chose to analyze the stretch response due to this loading condition because previous studies suggest that injuries most commonly occur in skeletal muscle during eccentric contractions (Armstrong et al., 1983; Faulkner et al., 1993; Lieber and Friden, 1993; Lieber and Friden, 2002; Noonan and Garrett, 1992; Schwane and Armstrong, 1983). All simulations were quasi-static, therefore dynamic effects were not considered.

We sampled the fiber maps (defined above) in several locations to obtain evenly distributed representative “fibers” that we could track throughout a simulation. The number of fibers remained the same for all iterations of the simple model. We calculated the along-fiber stretch (λ) distribution along the representative fibers for both the simple BFLH model and the MR-based BFLH model. The along-fiber stretch was defined as:

$$\lambda = \sqrt{\mathbf{a_o} \cdot \mathbf{C} \cdot \mathbf{a_o}} = \sqrt{I_4} \quad (3)$$

where $\mathbf{a_0}$ is a vector defining the fiber direction and **C** is the right Cauchy-Green deformation tensor (Holzapfel, 2000). A stretch value greater than 1 indicates lengthening while a value less than 1 indicates shortening. Along-fiber stretch values were sampled at fifty evenly distributed points along the length of each representative fiber in order to quantify how along-fiber stretch varies from the proximal attachment to the distal attachment of the muscle. Fiber stretch distributions on an element-by-element level were visualized using PostView (FEBio, MRL University of Utah).

Results

The MR-based model of the BFLH predicted non-uniform stretches throughout the muscle, which was demonstrated by both the element-by-element stretch analysis (Fig. 3) and the representative fiber analysis (Fig. 4). The element-by-element analysis demonstrated that the along-fiber stretch varied through the muscle cross-section, with peak values localized in the muscle tissue near the proximal MTJ. The representative fiber analysis demonstrated that the along-fiber stretch values were dependent on the region chosen for analysis and were generally largest near the proximal MTJ (Fig. 4). In order to quantify the distribution of stretches across representative fibers in the muscle, we separated the fibers into three regions as defined by the point of origin along the proximal aponeurosis (Fig. 4A). An average peak stretch of 1.64 ± 0.15 was predicted in the middle region of the muscle belly adjacent to the proximal MTJ (Fig. 4C).Stretches were slightly lower in the superior and inferior regions of the muscle with peak values of 1.21 ± 0.32 (Fig. 4B) and 1.54 ± 0.53 respectively (Fig. 4D). Therefore, we focused the remaining analyses of the MR-based model on fibers within the middle region because this region is the location of peak stretches in the model and is often associated with injury (Koulouris and Connell, 2003).

The average along-fiber stretch distribution for the simple model was similar to that described by the average curve for the middle region of the MR-based BFLH model (Fig. 5). The peak along-fiber stretch for both the simple BFLH model and the MR-based BFLH model occurred adjacent to the proximal MTJ. Additionally, both models predicted minimum stretches within the middle of the muscle belly with average stretches increasing slightly near the distal MTJ (Fig. 5).

Varying the aponeurosis width in the simple model had the greatest impact on the predicted stretch distributions (Fig. 6). The model with two identical aponeuroses (Variation I) predicted nearly uniform stretch distributions. The model in which the two aponeuroses had different widths (Variation II) predicted highly nonuniform stretches; stretches were high along the proximal MTJ and low along the distal MTJ. Differences in the external tendon and aponeurosis stretches between Variation I and Variation II do not explain the large predicted differences in peak local muscle fiber stretches between the models (Table 2). In fact, while the peak local fiber stretch was much greater in Variation II than Variation I, the average muscle fiber stretch was greater in Variation I than in Variation II.

When the difference in aponeurosis lengths is introduced (simple BFLH model), stretches slightly decreased along the proximal MTJ and increased along the distal MTJ (Fig. 6), as compared to Variation II. Varying aponeurosis thickness in the simple model impacted the average fiber stretches (Table 2), but had little impact on the distribution of stretch along the fibers (Fig. 7). The model in which the proximal aponeurosis thickness was decreased by 3-fold (Variation III) predicted stretches that were slightly lower than those predicted by the

simple model; however, the stretch distribution was similar. Conversely, increasing the thickness of the aponeuroses (Variation IV) increased the average stretches, but had little impact on the stretch distribution (Fig. 7).

Discussion

Previous investigations have found that the BFLH is the most commonly injured hamstring muscle during athletic activity (Connell et al., 2004; De Smet and Best, 2000; Orchard, 2001). Imaging studies of prior strain injuries have also found a larger percentage of injuries in the proximal region of the BFLH, particularly near the MTJ (De Smet and Best, 2000; Silder et al., 2008). The purpose of this study was to identify morphological parameters that may contribute to the presence and location of injury in the BFLH muscle. Our finite element model of the BFLH muscle predicted nonuniform stretches within the muscle, with largest stretches localized in the middle region of the muscle near the proximal MTJ during activated muscle lengthening. Furthermore, analysis of our models showed that the relative widths of the proximal and distal aponeuroses greatly affects how stretches are distributed within the muscle and provides a explanation for why the muscles are commonly injured near the proximal MTJ.

Our results suggest that muscles with one wide and one narrow aponeurosis are more susceptible to injury as opposed to muscles with two wide aponeuroses. Furthermore, we propose that injury will likely be localized along the MTJ at the narrow aponeurosis because strains will be localized within this region. Injury observations in other muscles have also found that injury occurs near the MTJ (Best et al., 1995; Garrett, 1990; Jarvinen et al., 2000; Noonan and Garrett, 1999). However, no studies have as of yet discussed what role the shape and geometry of the aponeuroses may play in the injury mechanism. Studies in the human rectus femoris muscle have found that injury is more common along the distal MTJ in the anterior portion of the muscle at the point of insertion into the quadriceps tendon (Hughes et al., 1995; Koulouris and Connell, 2006; Orchard, 2001). This muscle has a narrow anterior aponeurosis and broader posterior aponeurosis (Yang et al., 2006). Based on our results, this injury pattern may be explained by the aponeurosis morphology with injury more commonly occurring along the narrower aponeurosis due to higher local strains. Generally, our results demonstrate that it is valuable to consider the morphology of the aponeuroses in addition to standard architectural measurements when studying a muscle's injury susceptibility.

There are several limitations to this study. First, material parameters used in the constitutive model have not all been thoroughly determined through experimental tests. For example, the along-fiber shear modulus has not been experimentally measured for skeletal muscle fibers and connective tissue. However, strain predictions made by a model employing the same constitutive model and moduli used in the present study have been validated with strain measurements from imaging experiments in the biceps brachii muscle (Blemker et al., 2005). In order to understand how our results were affected by changes to the along-fiber shear properties, we conducted a sensitivity analysis in the MR-based BFLH model. Varying the along-fiber shear modulus by three orders of magnitude resulted in a similar stretch distribution with peak stretches located along the proximal MTJ in the middle region of the muscle. Due to the complexity of obtaining *in* vivo stretch measurements of muscle fibers undergoing active lengthening, the stretches predicted by this model have not been thoroughly validated with experimental data. However, the predictions made by the model agree well with the high incidence of proximal injuries observed in the BFLH (Askling et al., 2007; Clanton and Coupe, 1998; Koulouris and Connell, 2003; Silder et al., 2008). Furthermore, the goal of this work was to explore the effects of morphology in determining how strains are distributed throughout the muscle, not to report exact local strain values.

Second, there are several complex biological parameters that may affect our results, but are not currently included in our models. These include interactions between multiple muscles, interactions between muscles and connective tissues, and spatially variable activation levels. Previous work has shown that interactions between muscles and surrounding structures may affect strains within a muscle (Yucesoy et al., 2003) and that both activation levels and fascicle length changes can be spatially variable within a muscle (Higham et al., 2008). However, our models have shown that morphological complexity alone can result in substantial variation in strain throughout the muscle. In the future, the models should be further extended to include these other biological factors to explore how they may affect predicted strains in the BFLH muscle.

Third, the activation and muscle-tendon length change conditions performed in our simulations were relatively simple, as compared to the loading of the hamstrings during actual sprinting movements. Future work should study the effects of more complex loading associated with sprinting and also include the effects of all muscles within the hamstrings group. This could be done through coupling the FE simulations described in this work with a multibody simulation of sprinting (Thelen et al., 2005a).

While most studies have found the highest incidence of injuries in the proximal region of the BFLH (De Smet and Best, 2000; Silder et al., 2008), injuries still do sometimes occur in other regions of the muscle (Koulouris and Connell 2003). The results of our analysis provide an explanation for the prevalence of injuries near the proximal MTJ. However, it is probable that other factors such as morphological variability in aponeurosis geometry across individuals (which is currently unknown), interactions between muscles and connective tissues, and the more complex loading conditions associated with sprinting may contribute to the injuries observed in regions that are not near the proximal MTJ. A model that accounts for these additional factors is needed in order to explain why injuries occur in other regions of the BFLH muscle.

The results of our modeling analysis have inspired the formation of two new hypotheses regarding the relationship between aponeurosis dimensions and injury susceptibility: (i) the observed prevalence of injuries near the proximal MTJ in the BFLH is due to the fact that the proximal aponeurosis is much more narrow than the distal aponeurosis in this muscle, and (ii) the relative aponeurosis dimensions of the BFLH explain the observed prevalence of injuries in the BFLH as compared to other hamstrings muscles. These hypotheses lead to several questions. First, how variable are the BFLH aponeurosis widths across individuals and might some individuals have relative aponeurosis widths that make them more prone to injury than others? Second, do the aponeurosis dimensions of the BFLH differ from the other hamstrings muscles and might these differences explain why the BFLH is injured most frequently? Lastly, how do aponeurosis dimensions adapt to training and therapy, and can this information be used to provide targeted training to minimize injury susceptibly? The models presented in this study provide a new framework for analysis of skeletal muscle injuries that will hopefully lead to amore scientific basis for treating and preventing muscle strain injuries.

Acknowledgments

We are thankful to Darryl Thelen and Amy Silder from the University of Wisconsin-Madison. Funding for this work was provided by the National Institutes of Health Grant R01 AR 056201.

References

Armfield DR, Kim DH, Towers JD, Bradley JP, Robertson DD. Sports-Related Muscle Injury in the Lower Extremity. Clinics in Sports Medicine. 2006; 4:803–842. [PubMed: 16962427]

Armstrong RB, Ogilvie RW, Schwane JA. Eccentric exercise-induced injury to rat skeletal muscle. Journal of Applied Physiology. 1983; 1:80–93. [PubMed: 6826426]

Askling CM, Tengvar M, Saartok T, Thorstensson A. Acute first-time hamstring strains during high-speed running: a longitudinal study including clinical and magnetic resonance imaging findings. The American Journal of Sports Medicine. 2007; 2:197–206. [PubMed: 17170160]

Azizi E, Roberts TJ. Biaxial strain and variable stiffness in aponeuroses. Comparative Biochemistry and Physiology - Part A: Molecular & Integrative Physiology 2. 2009 Supplement 1:S128–S128.

Best TM, McElhaney JH, Garrett WE Jr, Myers BS. Axial strain measurements in skeletal muscle at various strain rates. Journal of Biomechanical Engineering. 1995; 3:262–265. [PubMed: 8618377]

Blemker S, Delp S. Three-dimensional Representation of Complex Muscle Architectures and Geometries. Annals of Biomedical Engineering. 2005; 5:661–673. [PubMed: 15981866]

Blemker SS, Pinsky PM, Delp SL. A 3D model of muscle reveals the causes of nonuniform strains in the biceps brachii. Journal of Biomechanics. 2005; 4:657–665. [PubMed: 15713285]

C. Criscione J, S. Douglas A, C. Hunter W. Physically based strain invariant set for materials exhibiting transversely isotropic behavior. Journal of the Mechanics and Physics of Solids. 2001; 4:871–897.

Clanton T, Coupe K. Hamstring strains in athletes: diagnosis and treatment. Journal of the American Academy of Orthopaedic Surgeons. 1998; 4:237–248. [PubMed: 9682086]

Connell DA, Schneider-Kolsky ME, Hoving JL, Malara F, Buchbinder R, Koulouris G, Burke F, Bass C. Longitudinal Study Comparing Sonographic and MRI Assessments of Acute and Healing Hamstring Injuries. American Journal of Roentgenology. 2004; 4:975–984. [PubMed: 15385289]

De Smet AA, Best TM. MR imaging of the distribution and location of acute hamstring injuries in athletes. AJR.American Journal of Roentgenology. 2000; 2:393–399. [PubMed: 10658712]

Faulkner JA, Brooks SV, Opiteck JA. Injury to skeletal muscle fibers during contractions: conditions of occurrence and prevention. Physical Therapy. 1993; 12:911–921. [PubMed: 8248299]

Garrett WE Jr. Muscle strain injuries: clinical and basic aspects. Medicine and Science in Sports and Exercise. 1990; 4:436–443. [PubMed: 2205779]

Garrett W. Muscle strain injuries. Journal of Science and Medicine in Sport 1. 1999 Supplement 1:39–39.

Higham TE, Biewener AA, Wakeling JM. Functional diversification within and between muscle synergists during locomotion. Biology Letters. 2008; 4:41–44. [PubMed: 17986428]

Holzapfel, GA. Nonlinear solid mechanics: a continuum approach for engineering. New York: Wiley; 2000.

Hughes C 4th, Hasselman CT, Best TM, Martinez S, Garrett WE Jr. Incomplete, intrasubstance strain injuries of the rectus femoris muscle. The American Journal of Sports Medicine. 1995; 4:500–506. [PubMed: 7573664]

Jarvinen TA, Kaariainen M, Jarvinen M, Kalimo H. Muscle strain injuries. Current Opinion in Rheumatology. 2000; 2:155–161. [PubMed: 10751019]

Koulouris G, Connell D. Evaluation of the hamstring muscle complex following acute injury. Skeletal Radiology. 2003; 10:582–589. [PubMed: 12942206]

Koulouris, G.; Connell, DA. Soft Tissue Injuries. Germany: Springer; 2006. p. 267-282.

Lemos RR, Epstein M, Herzog W. Modeling of skeletal muscle: the influence of tendon and aponeuroses compliance on the force-length relationship. Medical & Biological Engineering & Computing. 2008; 1:23–32. [PubMed: 17917756]

Lieber RL, Friden J. Mechanisms of muscle injury gleaned from animal models. American Journal of Physical Medicine & Rehabilitation / Association of Academic Physiatrists. 2002; 11 Suppl:S70–S79.

Lieber RL, Friden J. Muscle damage is not a function of muscle force but active muscle strain. Journal of Applied Physiology. 1993; 2:520–526. [PubMed: 8458765]

Noonan TJ, Garrett WE Jr. Muscle strain injury: diagnosis and treatment. The Journal of the American Academy of Orthopaedic Surgeons. 1999; 4:262–269. [PubMed: 10434080]

Noonan TJ, Garrett WE Jr. Injuries at the myotendinous junction. Clinics in Sports Medicine. 1992; 4:783–806. [PubMed: 1423698]

Orchard JW. Intrinsic and extrinsic risk factors for muscle strains in Australian football. The American Journal of Sports Medicine. 2001; 3:300–303. [PubMed: 11394599]

Puso, MA.; Maker, BN.; Ferencz, RM.; Hallquist, JO. Nike3d: A Nonlinear, Implicit, Three-Dimensional Finite Element Code for Solid and Structural Mechanics. Lawrence Livermore National Lab Technical Report; 2006.

Roberts TJ, Marsh RL, Weyand PG, Taylor CR. Muscular Force in Running Turkeys: The Economy of Minimizing Work. Science. 1997; 5303:1113–1115. [PubMed: 9027309]

Schwane JA, Armstrong RB. Effect of training on skeletal muscle injury from downhill running in rats. Journal of Applied Physiology. 1983; 3:969–975. [PubMed: 6629931]

Silder A, Heiderscheit B, Thelen D, Enright T, Tuite M. MR observations of longterm musculotendon remodeling following a hamstring strain injury. Skeletal Radiology. 2008; 12:1101–1109. [PubMed: 18649077]

Thelen D, Chumanov E, Best T, Swanson S, Heiderscheit B. Simulation of Biceps Femoris Musculotendon Mechanics during the Swing Phase of Sprinting. Medicine & Science in Sports & Exercise. 2005a; 11:1931–1938.

Thelen D, Chumanov E, Dina H, Best T, Swanson S, Li L, Young M, Heiderscheit B. Hamstring Muscle Kinematics during Treadmill Sprinting. Medicine & Science in Sports & Exercise. 2005b; 1:108–114.

Ward SR, Eng CM, Smallwood LH, Lieber RL. Are current measurements of lower extremity muscle architecture accurate? Clinical Orthopaedics and Related Research. 2009; 4:1074–1082. [PubMed: 18972175]

Weiss JA, Maker BN, Govindjee S. Finite element implementation of incompressible, transversely isotropic hyperelasticity. Computer Methods in Applied Mechanics and Engineering. 1996; 1–2:107–128.

Woodley SJ, Mercer SR. Hamstring Muscles: Architecture and Innervation. Cells Tissues Organs. 2005:125–141. [PubMed: 15947463]

Yang D, Morris SF, Tang M, Geddes CR. A modified longitudinally split segmental rectus femoris muscle flap transfer for facial reanimation: anatomic basis and clinical applications. Journal of Plastic, Reconstructive & Aesthetic Surgery : JPRAS. 2006; 8:807–814.

Yucesoy CA, Koopman BHFJM, Baan GC, Grootenboer HJ, Huijing PA. Effects of inter- and extramuscular myofascial force transmission on adjacent synergistic muscles: assessment by experiments and finite-element modeling. Journal of Biomechanics. 2003; 12:1797–1811. [PubMed: 14614933]

Zajac FE. Muscle and tendon: properties, models, scaling, and application to biomechanics and motor control. Critical Reviews in Biomedical Engineering. 1989; 4:359–411. [PubMed: 2676342]

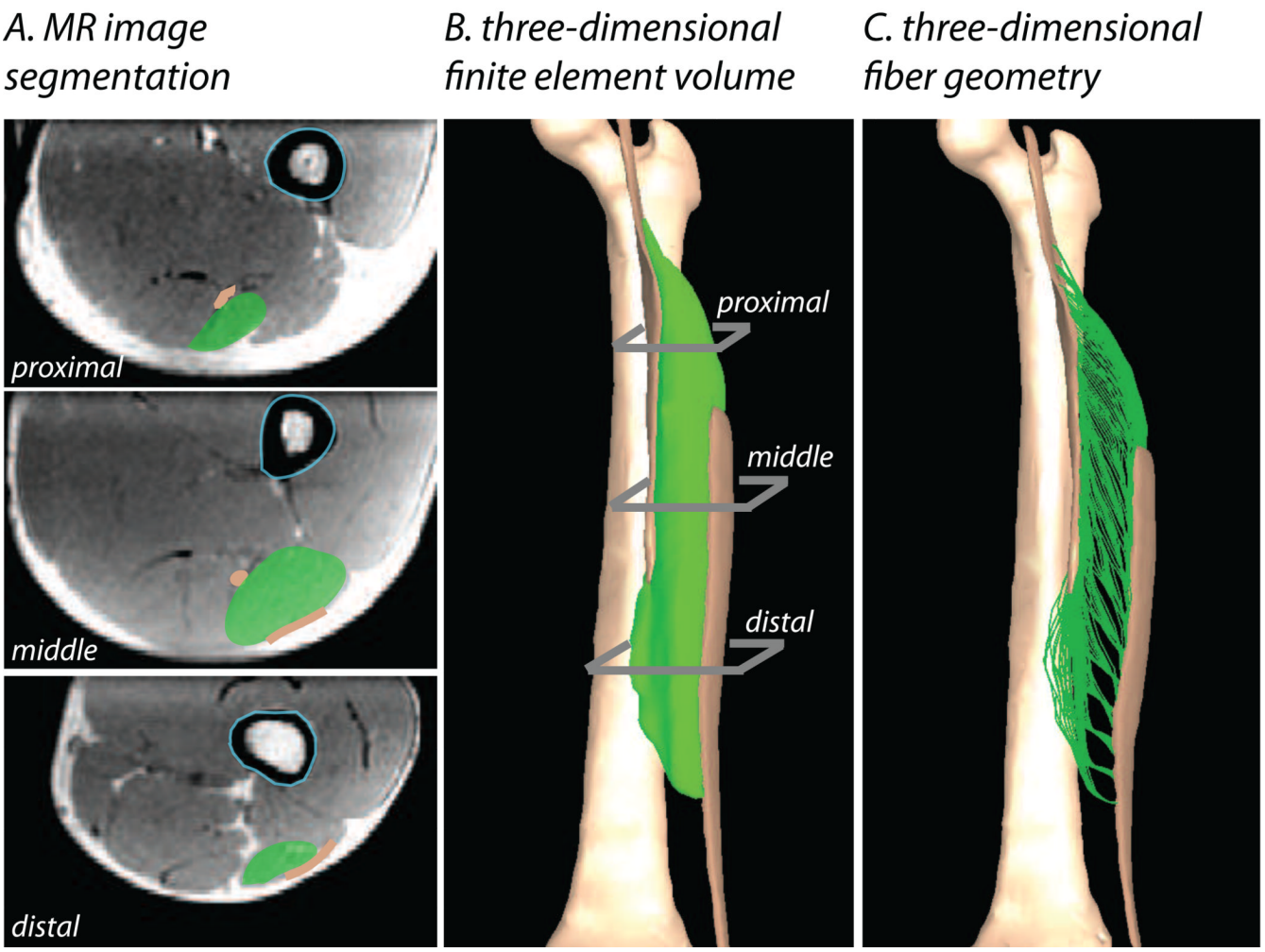

Figure 1.
Methods for constructing three-dimensional finite elements models of the BFLH. Models were built from axial magnetic resonance images of the thigh (A). The BFLH (green shaded regions), aponeuroses (brown shaded regions), and femur (light blue outline) were manually outlined in each image. Finite-element meshes (B) of the BFLH and aponeuroses were created from the series of outlines. A representation of the three-dimensional trajectories of fibers (C) was created using a fiber mapping technique.

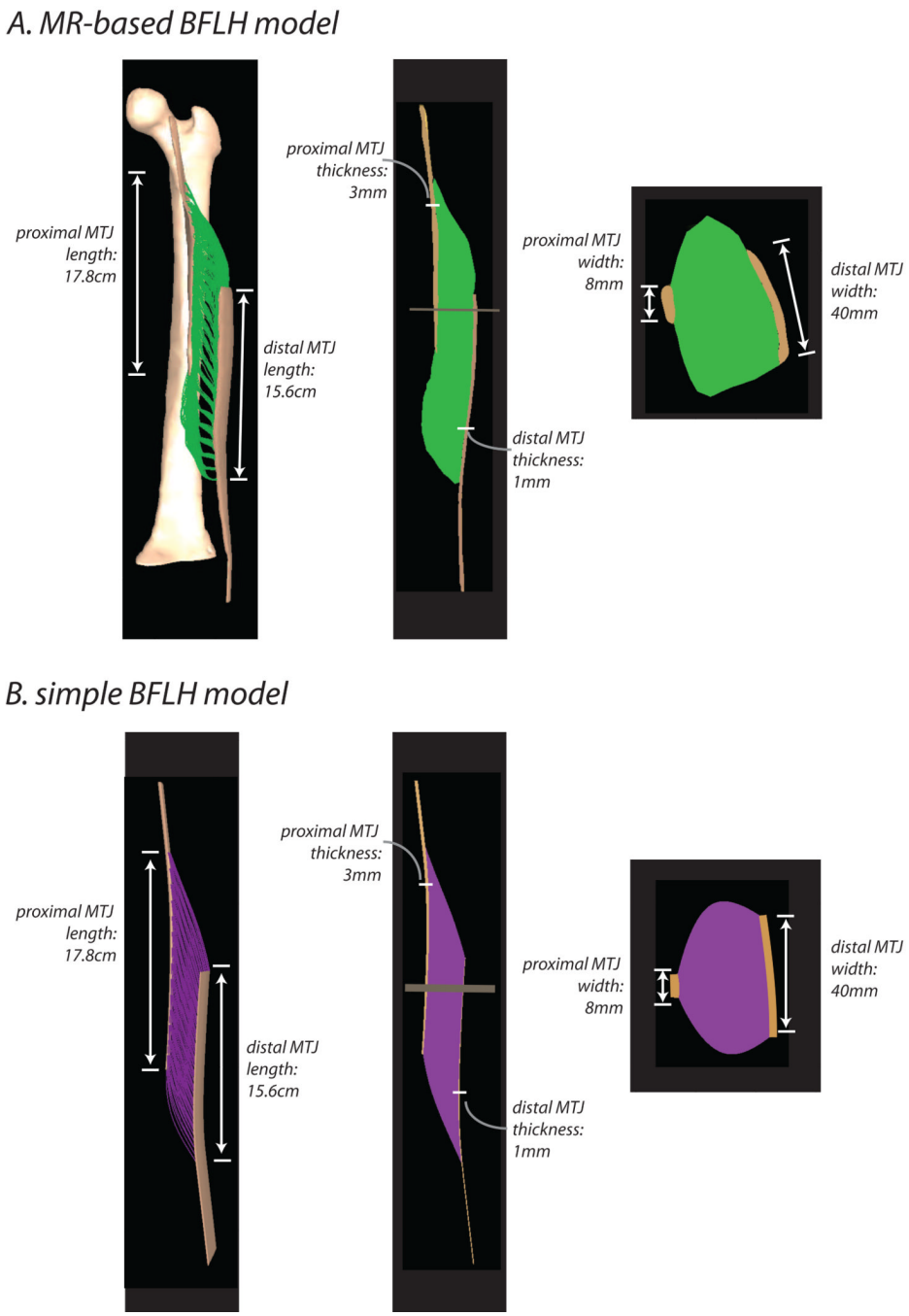

Figure 2.

Description of aponeurosis dimensions. Aponeurosis length, thickness, and width were measured on the MR based model (A). The measurements from the MR based model were used to define the aponeurosis morphology in the simple BFLH model (B). Variations on the simple BFLH model were created by varying the aponeurosis length, thickness, and width.

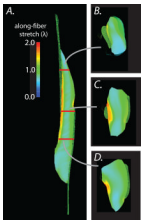

Figure 3.
Along-fiber stretch distribution in the MR-based model, analyzed on the element-by-element level. A lengthening contraction was simulated and the resulting distribution of along-fiber stretch was studied in an oblique coronal cross section (A) and three representative axial cross sections (B–D).

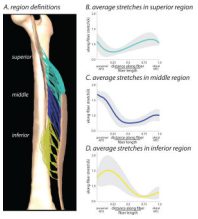

Figure 4.

Regional BFLH stretch distribution, analyzed for representative fibers across the muscle. In order to quantify the stretch distribution across fibers throughout the whole muscle volume, the muscle was divided into three separate regions: superior, middle, inferior (A). We calculated the along-fiber stretch distribution along the representative fibers within each region in the model. The average (± one standard deviation) along- fiber stretch for each region was plotted vs. the normalized distance along the fiber (B–D).

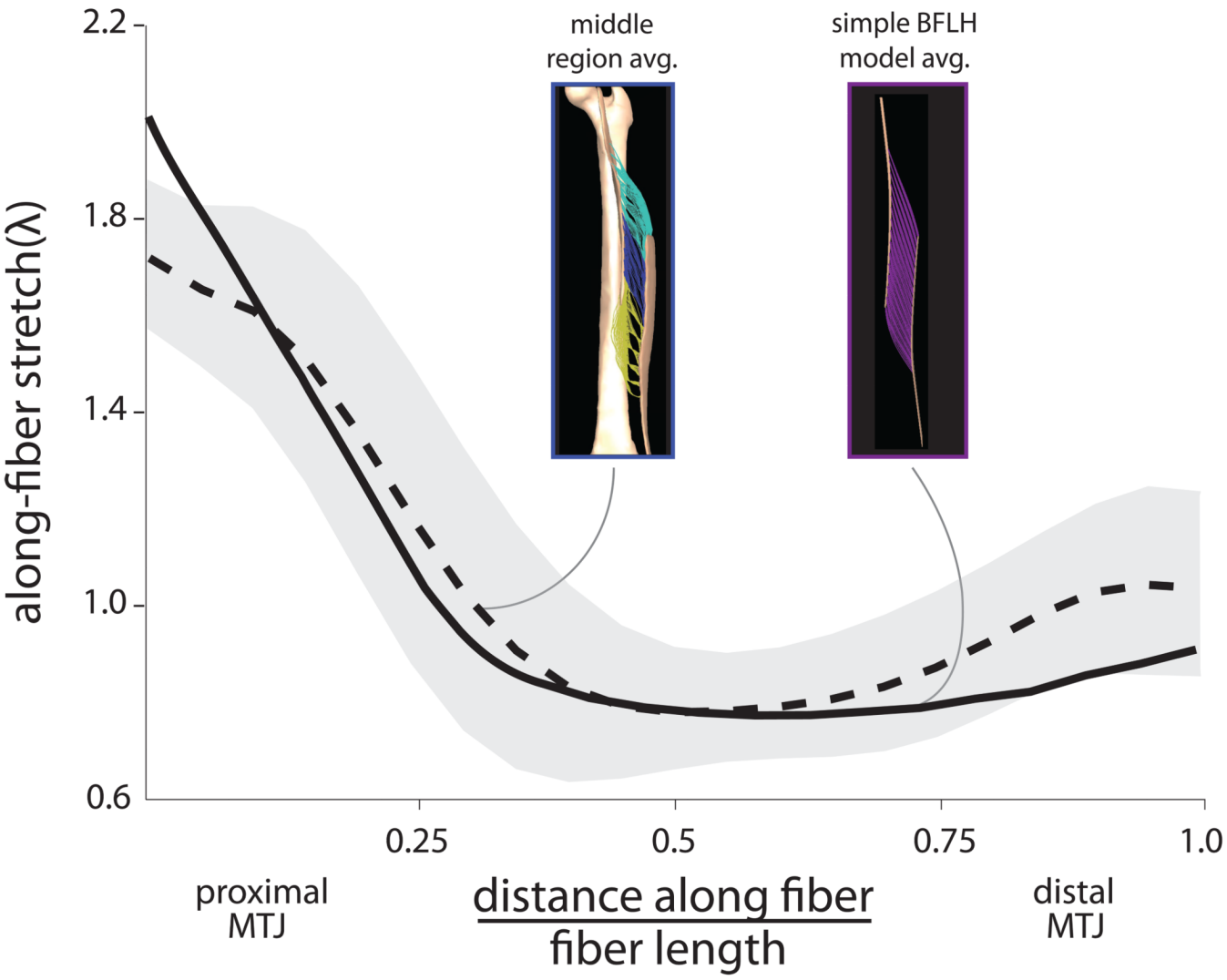

Figure 5.
Comparison of the MR-based model and the simple BFLH model. The along-fiber stretch distribution from the middle region of the MR based model was compared to the average predicted along–fiber stretch in the simple BFLH model.

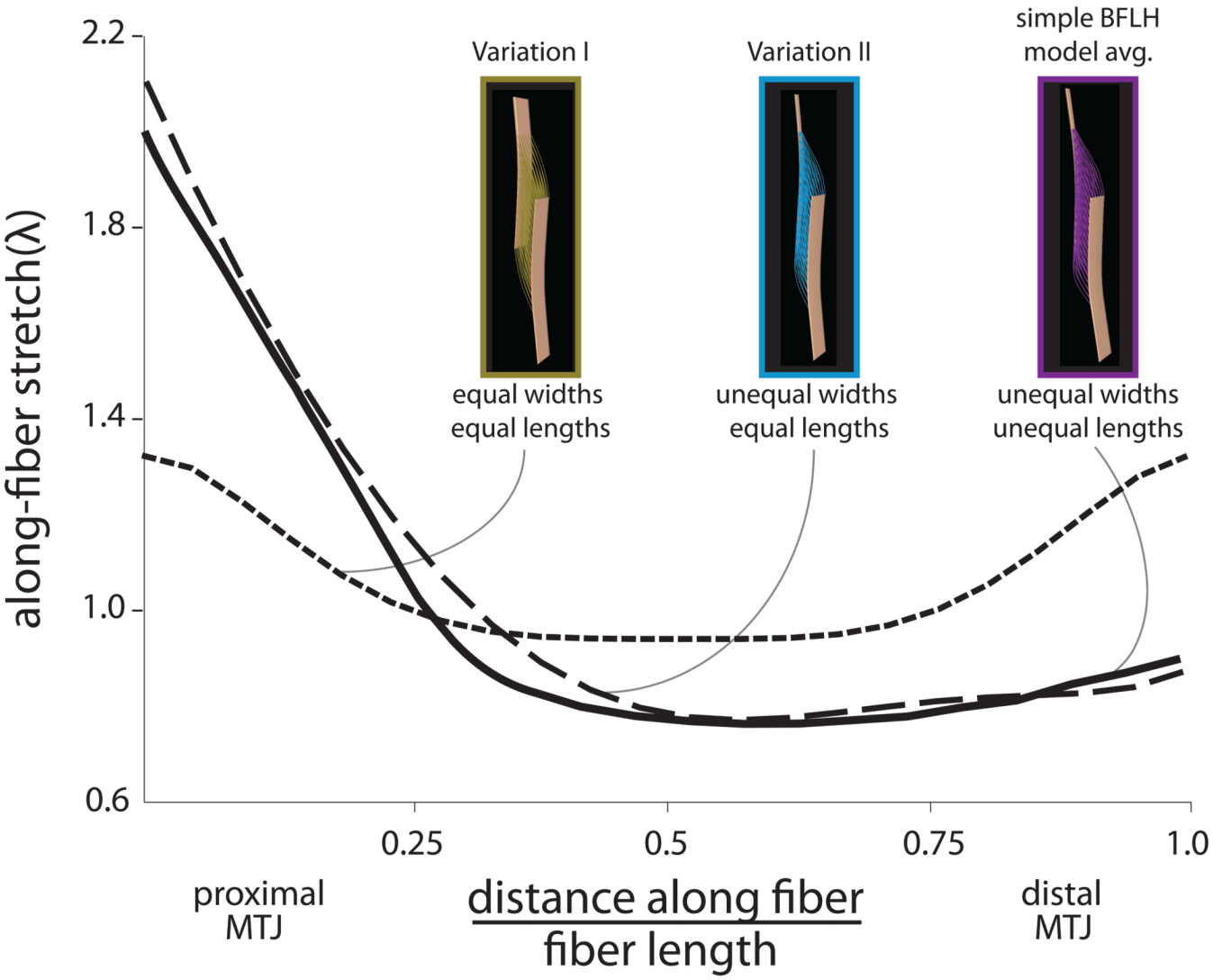

Figure 6.
Effects of aponeurosis length and width. The simple model with equal aponeurosis widths and equal lengths (Variation I) predicted nearly uniform stretch distributions. Decreasing the width of the proximal aponeurosis (Variation II) substantially increased the stretches along the proximal MTJ. Comparing Variation II and the simple BFLH model showed that shortening the distal aponeurosis slightly decreased the stretches along the proximal aponeurosis and increased stretches along the distal aponeurosis.

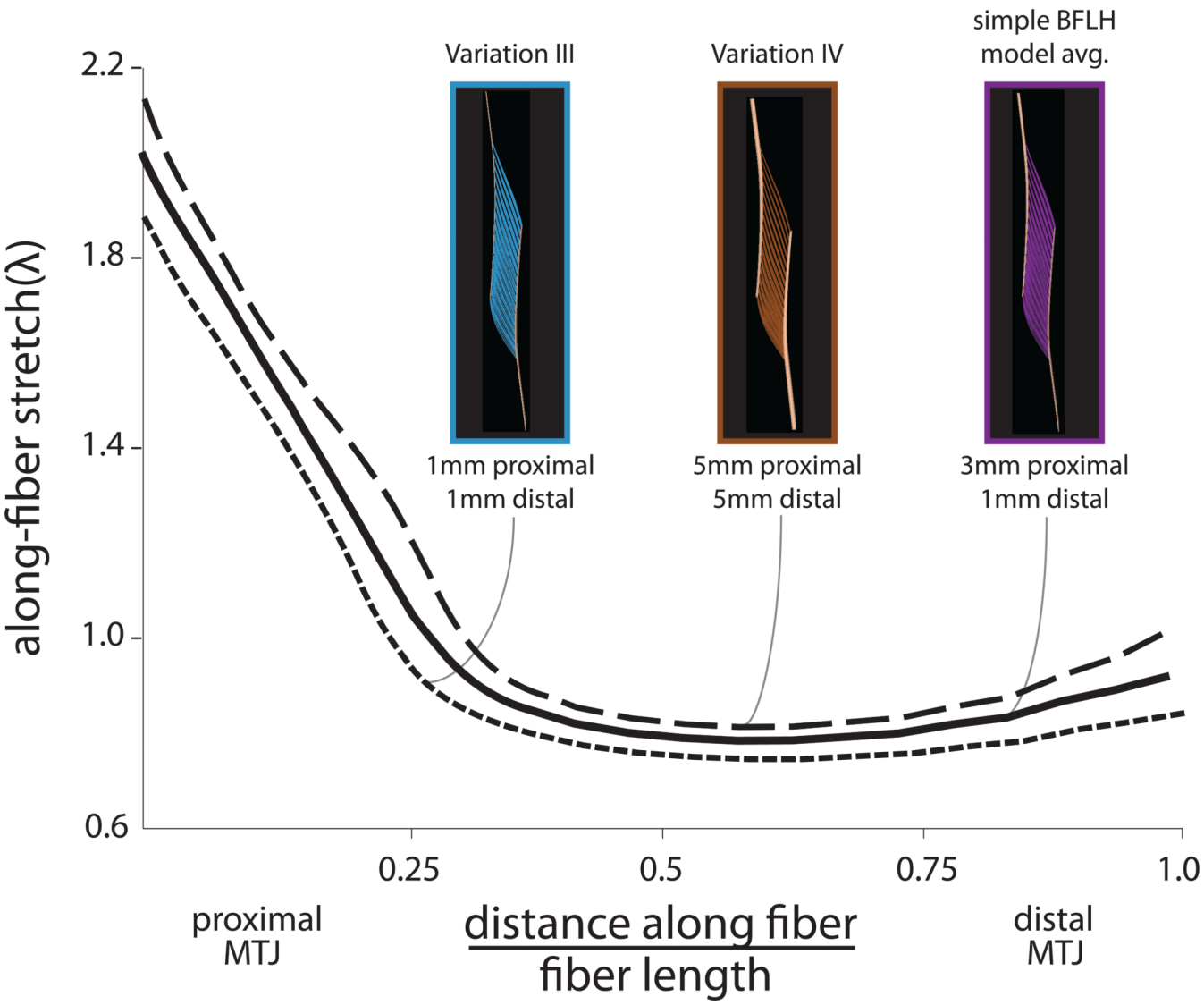

Figure 7.
Effects of aponeurosis thickness. Decreasing the thickness of both aponeuroses (Variation III) decreased the stretches along the entire length of the muscle fiber. Conversely, increasing the thickness of the aponeuroses (Variation IV) increased the stretches along the length of the fiber.

Table 1

		Width (mm)	Length (cm)	Thickness (mm)
Variation I	proximal aponeurosis	40	17.8	3
	distal aponeurosis	40	17.8	1
Variation II	proximal aponeurosis	8	17.8	3
	distal aponeurosis	40	17.8	1
Variation III	proximal aponeurosis	8	17.8	1
	distal aponeurosis	40	15.6	1
Variation IV	proximal aponeurosis	8	17.8	5
	distal aponeurosis	40	15.6	5
Simple BFLH	proximal aponeurosis	8	17.8	3
	distal aponeurosis	40	15.6	1

Table 2

	Average Proximal External Tendon Stretch	Average Proximal Aponeurosis Stretch	Average Distal External Tendon Stretch	Average Distal External Aponeurosis Stretch	Average Muscle Fiber Stretch
Variation I	1.022	1.015	1.047	1.032	1.063
Variation II	1.055	1.040	1.037	1.026	1.025
Variation III	1.129	1.083	1.034	1.024	0.950
Variation IV	1.041	1.033	1.015	1.007	1.072
Simple BFLH	1.056	1.042	1.038	1.026	1.023
MR-Based BFLH	1.035	1.019	1.005	1.021	1.027